JOURNAL OF CHEMICAL INFORMATION AND MODELING

Article

pubs.acs.org/jcim

Engineering Antimicrobial Peptides with Improved Antimicrobial and Hemolytic Activities

Jun Zhao,[†] Chao Zhao,[†] Guizhao Liang,[†,§] Mingzhen Zhang,[†] and Jie Zheng*[,†]

[†]Department of Chemical and Biomolecular Engineering, The University of Akron, Akron, Ohio 44325, United States

[§]Key Laboratory of Biorheological Science and Technology Ministry of Education, Bioengineering College Chongqing University, Chongqing 400044, P.R. China

Supporting Information

ABSTRACT: The rapid rise of antibiotic resistance in pathogens becomes a serious and growing threat to medicine and public health. Naturally occurring antimicrobial peptides (AMPs) are an important line of defense in the immune system against invading bacteria and microbial infection. In this work, we present a combined computational and experimental study of the biological activity and membrane interaction of the computationally designed Bac2A-based peptide library. We used the MARTINI coarse-grained molecular dynamics with adaptive biasing force method and the umbrella sampling technique to investigate the translocation of a total of 91 peptides with different amino acid substitutions through a mixed anionic POPE/POPG (3:1) bilayer and a neutral POPC bilayer, which mimic the bacterial inner membrane and the human red blood cell (hRBC) membrane, respectively. Potential of mean force (PMF, free energy profile) was obtained to measure the free energy barrier required to transfer the peptides from the bulk water phase to the water−membrane interface and to the bilayer interior. Different PMF profiles can indeed identify different membrane insertion scenarios by mapping out peptide−lipid energy landscapes, which are correlated with antimicrobial activity and hemolytic activity. Computationally designed peptides were further tested experimentally for their antimicrobial and hemolytic activities using bacteria growth inhibition assay and hemolysis assay. Comparison of PMF data with cell assay results reveals a good correlation of the peptides between predictive transmembrane activity and antimicrobial/hemolytic activity. Moreover, the most active mutants with the balanced substitutions of positively charged Arg and hydrophobic Trp residues at specific positions were discovered to achieve the improved antimicrobial activity while minimizing red blood cell lysis. Such substitutions provide more effective and cooperative interactions to distinguish the peptide interaction with different lipid bilayers. This work provides a useful computational tool to better understand the mechanism and energetics of membrane insertion of AMPs and to rationally design more effective AMPs.

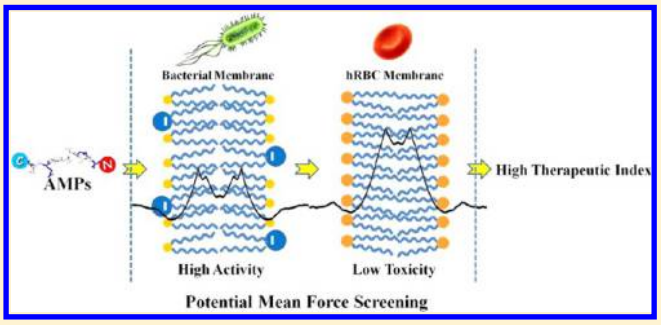

1. INTRODUCTION

Widespread use of antibiotics and infiltration of antibiotics into the food chain have promoted the enormous and growing threat of bacterial pathogens that have developed multidrug resistance (MDR) to almost all available antibiotics due to natural evolution, consequently causing many human infectious diseases such as urinary tract infections, tuberculosis, gastroenteritis, pneumonia, and wound infections.[1−3] Traditional antimicrobial drugs mainly consist of antibiotics and antimicrobial peptides (AMPs). A large number of antibiotics has been contemplated and widely used as FDA-approved drugs such as penicillins, polymyxins, quinolones, tetracylines, and sufonamides.[4,5] But, conventional antibiotics often suffer from the limited activity to kill both Gram-positive and Gram-negative pathogens and undesirable side effects. On the other hand, naturally occurring AMPs produced by mammals and plants offer many advantages as a next generation of "nature antibiotics,"[6−10] including broader spectrum activity to kill both Gram-positive and Gram-negative bacteria, fungi, and parasites (even clinically common methicillin-resistant *S. aureus* and vancomycin-resistant *Enterococcus*); a lower toxicity to host eukaryotic cells; and a synergistic and benign effect with conventional antibiotics.[1,11] Meanwhile, many bacteria have also developed resistance to almost all available antibiotics and AMPs to some degree via natural evolution.[3,12,13] Undoubtedly, there is an urgent need for the development of new effective AMPs to fight against accelerating bacteria MDR by natural evolution.

Generally, AMPs display high diversity in size (8−50 residues), sequences (overall positive charge and high population of hydrophobic residues), and structures (α-helical, β-stranded, β-hairpin, and extended structures).[14] AMPs mainly achieve their functions to kill invading bacteria, fungi, or viruses via a nonreceptor mediated mechanism of cell membrane disruption.[3,15,16] Interactions between AMPs and lipid bilayers

Received: August 12, 2013
Published: November 27, 2013

have been extensively studied by numerous methods including NMR,[17−21] sum frequency generation (SFG) vibrational spectroscopy,[22,23] circular dichroism,[24−26] membrane partition ability evaluation,[27−31] and molecular dynamics.[32−36] However, it still remains unclear fundamentally how AMPs interact with a cell membrane to induce membrane disruption. Depending on intrinsic physicochemical properties of AMPs such as size, sequence, structure, and charge distribution and environmental properties such as AMP concentrations, bacteria types, and membrane compositions, AMPs act differently at the membrane to induce different membrane disruptions. AMPs can insert into the cell membranes to form "barrel-stave" or "toroidal" transmembrane pores. The barrel-stave and toroidal structures are fundamentally different: in the barrel-stave pore, AMPs align vertically and parallel with respect to each other to form a circular pore, while in the toroidal pore, AMPs induce a local curvature of the lipid bilayer to form a highly curved pore. Apart from the transmembrane pore models, AMPs act as "detergents" to distract lipids from the membrane ("detergent model") or intensively adsorb onto and completely/partially insert into the membrane to induce changes in membrane permeability and integrity ("carpet" model). Combinations of these models have also been proposed.[37] All of these models above could cause similar membrane disruption, leakage of cytoplasmic contents, and concomitant bacterial cell death.[16]

Because of their peptidic nature, most natural AMPs suffer from poor bioavailability and poor proteolytic stability, which limits their therapeutic applications.[8] It is often necessary to (i) explore a vast population of diverse chemical and biochemical sequences from other protein/peptide families to increase sequence diversity and (ii) introduce un-natural, D-amino acids or β-amino acids via point mutations and appropriate chemical modifications to improve proteolytic stability.[3,38] The modified AMPs tend to enhance their interactions with cell membranes by facilitating themselves to attach on or insert into the membranes. Apart from bioavailability and stability issues of AMPs, cell selectivity is another major concern for rational design of effective AMPs. Strong membrane binding and insertion ability of AMPs to bacteria could also give rise to human red blood cells, resulting in lysis of human red blood cells via similar membrane-disruption mechanisms. Considering that the structural features common to many AMPs are the presence of cationic and hydrophobic residues,[39−43] it is reasonable to speculate that cell selectivity of AMPs could be improved by tuning the composition, position, and ratio of cationic and hydrophobic residues; i.e. balancing the cationic charge and hydrophobicity of AMPs is requisite to obtain nontoxic antimicrobial peptides, which are expected to kill bacteria efficiently while minimizing harm to human cells. Generally speaking, cationic residues of AMPs enhance the specificity of their binding to bacterial cell membranes relative to human cell membranes, because the former contain a greater amount of anionic lipids on the outer leaflet.

Because of the promising activity of AMPs as a substitute of traditional antibiotics, extensive studies have been conducted to screen and design potent AMP candidates using different high-throughput screening methods. These methods include virtual screening, phage-display library, solid-phase synthesis on arrays, and rapid luminescence-based assay for bacterial killing,[8,44] which lead to the establishment of several AMP databases including the Antimicrobial Peptides Database (APD)[45] and Collection of Anti-Microbial Peptides (CAMP).[46] However, most peptides in the databases have the disadvantage of inconsistent activity data of either MIC or IC_{50}, and such discrepancy is very likely caused by different experimental conditions, which make it more difficult to accurately establish the sequence−activity relationships of AMPs. It is thus desirable to use a more reliable data set as model systems to better understand the mechanism of AMPs.

A bovine dodecapeptide variant (Bac2A, RLARIVVIRVAR-NH_2)[47,48] is one of the smallest natural occurring antimicrobial peptides. Bac2A has modest activity against Gram-negative bacteria and higher activity against Gram-positive bacteria. Hilpert et al. performed a complete single-point substitution library of Bac2A ($12 \times 19 = 228$) for determining the position importance of specific amino acids in Bac2A and the antimicrobial activity of mutated sequences using a high-throughput cellulose synthesis method.[49] Among 228 substitutions, 46 peptides (~20%) showed improved activity and 52 peptides (~22%) showed equivalent activity to the parent Bac2A peptide, as demonstrated by low IC_{50} and MIC values. This complete substitution library of 12-amino-acid peptides based on Bac2A provides an excellent model system for computationally probing the sequence−structure activity of AMPs and for rationally designing new AMPs with improved antibiotic activity.

The Bac2A-based peptide library is homogeneous, as all peptides were assayed under the same conditions, and thus is of great value to testing the sequence−activity relationship in this study. It is an extremely challenging task to study the interactions or insertion of the peptides into a membrane with sufficient temporal and spatial resolution experimentally. Conventional molecular dynamics (MD) simulations are also not expected to observe the spontaneous translocation of the peptides across the membrane due to limited time and length scales, unless advanced simulation techniques and nonphysical restraints are applied to accelerate the peptide penetration process. Here, we developed an integrated platform combining potential of mean force molecular dynamics (PMF-MD) simulations and experimental tests to probe an interaction model of AMPs with a mixed anionic POPE/POPG bilayer with a ratio of POPE/POPG = 3:1 and a neutral POPC bilayer. The mixed POPE/POPG bilayer mimics the bacterial cytoplasmic membrane, while the neutral POPC bilayer mimics the human red blood cell (hRBC) membrane. The partition of AMPs into different lipid bilayers produced different PMF profiles, which help to determine insertion free energy barriers and to predict both antibacterial and hemolytic activities of AMPs. PMF-MD results indicated that antimicrobial activity is closely related to the trans-membrane ability, which can be used to evaluate the antimicrobial activity of AMPs. Moreover, some AMPs with high antimicrobial activity also showed low hemolytic activity to the human red blood cell membrane. Throughout this straightforward and robust platform, peptides designed and selected by PMF-MD simulations displayed a favorable combination of effective antimicrobial activity and low hemolytic properties *in vitro*. This work provides valuable insights into the mechanism of both activity and selectivity of AMPs underlying peptide−membrane interactions at the atomic level. Moreover, the proposed platform, with potential application to high-throughput screening approaches, can also be generally applicable to evaluate the membrane activity of other membrane-associated peptides such as amyloid peptides and cell penetrating peptides.

2. MATERIALS AND METHODS

In general, spontaneous translocation of a peptide across the lipid bilayer is difficult to capture by the conventional all-atom MD simulations due to limited time and length scales. Herein, we applied three advanced computational techniques to overcome this obstacle: First, coarse-grained AMP-membrane systems were constructed to reduce the size and freedom of the modeling systems. Second, the adaptive biasing force (ABF) method was applied to drag and facilitate the AMPs for membrane translocation. Third, the umbrella sampling technique was applied to enhance the sampling of conformations and to obtain the potential of mean force upon AMP penetration into the membrane. Moreover, the results from the coarse-grained force field were validated by the united-atom force field, and further bacterial inhibition and hemolytic assays were performed to test computational results.

2.1. Coarse-Grained AMPs and Lipid Bilayers. The coarse grained (CG) simulations in this study were performed with the GROMACS simulation package 4.0.5.[50] Generally, phosphatidylethanolamine (PE) and phosphatidylglycerol (PG) are the major lipid components of bacterial membranes with a molar ratio of 3:1,[51] while phosphatidylcholine (PC) is the major lipid component of normal cell membranes.[52] To construct the bacterial- or red-blood-cell-mimic lipid bilayers, we randomly put 156 POPE/52 POPG lipids or 208 POPC lipids into a simulation box containing 1664 water molecules with an 8:1 ratio of water/lipids, and then we performed a series of self-assembly MD simulations allowing to spontaneously form a POPE/POPG or POPC lipid bilayer using a similar simulation protocol to that in our previous works.[53−56] Atomistic structures of the peptides were generated using the MEMSAT program,[57,58] followed by the conversion of atomic structure into CG structure using the CG protocol, parameters, and simulations as proposed by Marrink and co-workers.[59]

2.2. Adaptive Biasing Force (ABF) Method for Membrane Insertion. To construct the peptide-bilayer system, a single peptide was initially placed at 40 Å above the lipid bilayer with either C-terminal or N-terminal vertically orientating toward the bilayer. The peptide-bilayer system was then solvated in a polarizable water box. Counter ions of NaCl were added to achieve an electrical neural system with an ion strength of ∼100 mM. The resulting systems were subject to 10 000 steps of steepest descent minimization with position constraints on heavy atoms of the peptide, followed by an additional 10 000 steps of conjugate gradient minimization with position constraint of the peptide as well. To facilitate the peptide penetration process across the bilayer, a harmonic potential with a force constant of 1000 kJ/(mol nm^2) was applied to the center of mass (COM) of the peptide to pull the peptide across the bilayer along the Z axis. Additionally, to validate the models, two different spring constants of 900 and 1100 kJ mol^{-1} nm^{-2} were used for selected AMPs. Each peptide-lipid system was repeated by two independent ABF simulations with different initial velocities for all atoms.

2.3. Umbrella Sampling for PMF Profiles. To determine the free energy profile during the peptide penetration process, PMFs were calculated using the umbrella sampling protocol[60] as a function of the distance between the COM of the peptides and the lipid bilayer. The initial separation distance between the center of mass of peptides and the center of the bilayer was 4 nm. An asymmetric distribution of sampling windows was used. The window spacing was set to 0.1 nm between Z = 0 and 2 and 0.2 nm between Z = 2 and 4 nm, resulting in 31 windows. Such window spacing assignment allows one to obtain the more detailed energetic information on the peptide particularly within and near the lipid bilayer. van der Waals (VDW) interactions were calculated by the switch function with twin-range cutoff distances of 9 and 12 Å, while long-range electrostatic interactions were calculated by the particle-mesh Ewald (PME) method with a grid size of 1 Å and a real-space cutoff of 12 Å. Molecular dynamics (MD) simulations were performed using the NPT ensemble (constant pressure, temperature, and number of particles). The temperature was kept constant for each system at 310 K using the Berendsen thermostat[61] with a relaxation time of 1 ps. The pressure of the system is semi-isotropically coupled and maintained at 1 bar using the Berendsen algorithm with a time constant of 5 ps and a compressibility of 4.5 × 10^{-5} bar^{-1}.[61] A 25 fs time-step was used in the velocity Verlet integration. Each window was simulated for 100 ns to achieve adequate sampling of configurations under the biasing potential of 1000 kJ mol^{-1} nm^{-2} applied to restrain the COM of the peptides at a required distance from the center of the bilayer. Thus, obtaining a single PMF (free energy) profile requires 31 simulations up to a total of 3.1 μs, covering an entire translocation process. To obtain the unbiased PMFs, the weighted histogram analysis method (WHAM)[60] was used, with 200 bins and a tolerance of 10^{-5} kT, for window offsets. PMFs were converged with respect to the number of simulation windows and equilibration time, as established by block analysis (g_wham module in the GROMACS),[62] where PMF curves calculated over the two neighboring windows were overlapped by ∼50%.

2.4. United-Atom Models. To further validate the accuracy of the coarse-grained models, atomistic MD simulations of the wild type Bac2A sequence (both C-terminal and N-terminal insertion) were performed using a GROMACS united-atom (ffgmx) force field.[50] The atomistic structures of the AMP and lipid bilayer were reconstructed from coarse-grained structures using the structural conversion method as described by Rzepiela et al.,[63] followed by 20 000 steps of the steepest descent method for energy minimization. Then, atomic ABF-MD simulations with constant pressure, temperature, and number of particles (NPT ensemble) were performed. The temperature of 310 K was kept constant using a Berendsen thermostat with a relaxation time of 1 ps.[61] The pressure of the system was semi-isotropically coupled and maintained at 1 bar using a Berendsen algorithm with a time constant of 5 ps and a compressibility of 4.5 × 10^{-5} bar^{-1}.[61] The nonbonded potential energy functions were cut off and shifted at 12 Å, with forces smoothly decaying between 9 and 12 Å for van der Waals forces and throughout the whole interaction range for the treatment of electrostatic forces. The simulations were performed using a 2 fs integration time step. A 200 ns production MD simulation was performed for each window (total 31 windows), leading to a total ∼6.2 μs of united-atom MD simulation. The PMF profile was calculated using the same strategy as described in the coarse-grained models.

2.5. Bacteria Growth Inhibition Assay. *P. aeruginosa* PAO1 was cultured in separate agar plates overnight at 37 °C in trypticase soy broth (TSB; BD, Franklin Lakes, NJ). Several colonies of *P. aeruginosa* PAO1 were inoculated in 5 mL of TSB medium (10 g/L) at 37 °C under a 280 rpm shaking for 18 h. The received bacteria suspension was then diluted with a TSB medium to reach an optical density (OD) of 0.01 at 600 nm (OD600 = 1 ≈ 109 cells/mL culture) as measured by a

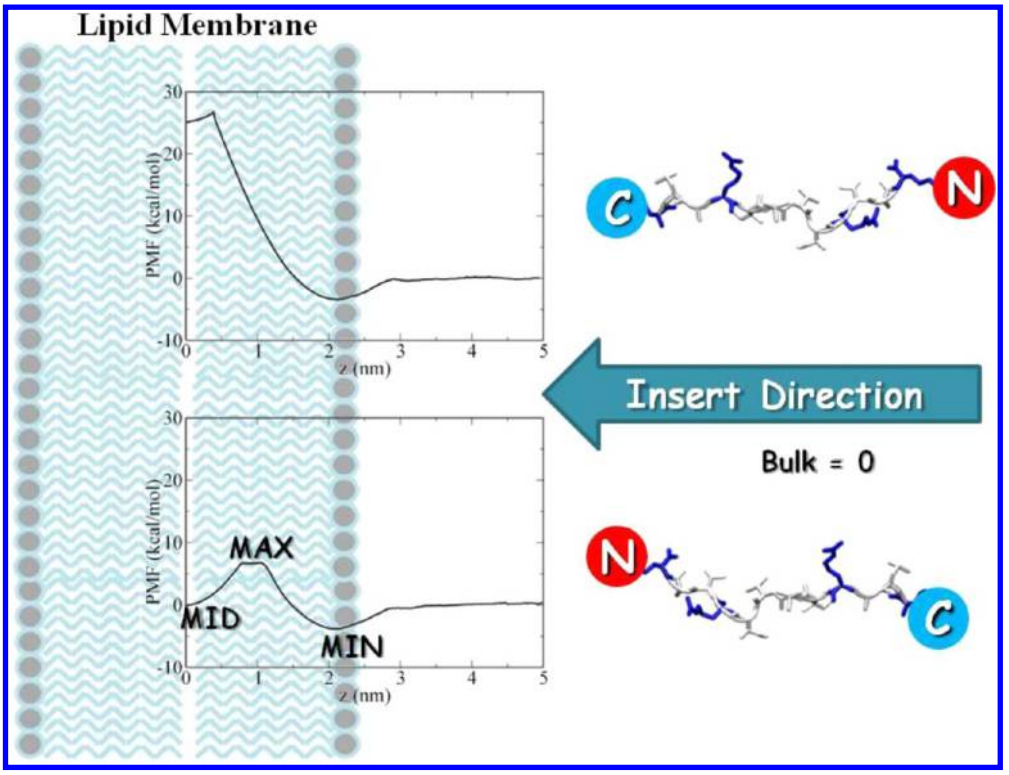

Figure 1. Schematic of membrane penetration of a given peptide with different C-/N-terminus insertion pathways. The partition of AMPs into different lipid bilayers produced different PMF profiles with three distinct MID, MAX, and MIN values, which help to determine insertion free energy barriers and to predict both antibacterial and hemolytic activities of AMPs.

spectrophotometer (Smartspet 300, Biorad, CA). A peptide stock solution of 1 mg/mL was prepared by dissolving peptides in a TSB medium; the sample was mixed by inversion to ensure peptides were completely dissolved in the TSB medium. To examine the growth inhibition property of peptides, 2 mL of prepared bacteria suspension with an OD600 of 0.01 were placed into individual wells of a sterile 24-well plate in triplicate, followed by the addition of a calculated volume of peptide solutions to each well for incubation at 37 °C for 24 h. After incubation, the bacteria suspensions were carefully removed from each well, and the OD600 of suspensions was measured by a spectrophotometer.

2.6. Hemolysis Assay. Samples were prepared within 3 h of performing the assay. Peptide stock solutions of 100 μg/mL were prepared by dissolving peptides in PBS (10 mM phosphate buffer, pH 7.4); the samples were mixed by inversion to ensure peptides were completely dissolved in PBS. To prepare the Human Red Blood Cell (hRBC) solution, 0.4 mL of fresh hRBC used as received (Cat. No: 991-09) from Lee Biosolutions, Inc. was rinsed two times with 7 mL of PBS by centrifugation for 10 min at 2500 rpm, and the precipitates were resuspended in 4 mL of PBS. To examine the hemolysis property of peptides, 1.6 mL of freshly prepared peptide solutions was mixed with 0.4 mL of freshly prepared hRBC solution by inversion and was placed in a water bath at 37 °C for 1 h. A total of 1.6 mL of PBS buffer only and 1.6 mL of Triton X-100 1% (w/v) were mixed with 0.4 mL of hRBC solution as negative and positive controls, respectively. After 1 h of incubation, all samples were centrifuged at 2500 rpm for 10 min. A total of 1 mL of supernatant was collected, and the release of hemoglobin was monitored by measuring the absorbance of the supernatant at 540 nm with a UV−vis instrument at 25 °C with the PBS buffer at the same pH as the blank. The percent hemolysis was calculated as the following equation.

$$\%\text{hemolysis} = \frac{\text{absorbance}_{\text{sample}} - \text{absorbance}_{\text{negative}}}{\text{absorbance}_{\text{positive}}} \times 100$$

3. RESULTS AND DISCUSSION

3.1. Model Validation for the Partition of AMPs into Lipid Bilayer. We have simulated a complete penetration process of AMP across a lipid bilayer and consequently obtained the free energy landscape along a penetration pathway using the MARTINI coarse-grained molecular dynamics (CG-MD).[64,65] The MARTINI CG-MD method is one of the most common CG methods for a wide range of simulations of proteins and membranes.[66,67] It can reproduce the accurate dynamic behavior of lipid bilayers and can be used to explore interactions between peptides and membranes at much longer time and length scales, which are hardly accessed by all-atom MD simulations. Atomic structures of Bac2A and its mutants were not reported experimentally, but circular dichroism (CD) showed that Bac2A adopted a random coil structure in bulk solution.[68] We used the MEMSAT program,[57,58] which is specifically developed for predicting the 3D structure of membrane proteins, to predict 3D atomic structures of Bac2A-based peptides, in which their secondary structures were predicted to be dominated by random coil structures.

In the Bac2A-based peptide library, we first selected wild type and 19 single-point mutation sequences of Bac2A, which covers a wide range of IC_{50} values from 0.03 to 0.75 and mutation sites by 11 different amino acids, to computationally examine the correlation between experimentally determined antimicriobial activities (IC_{50}) and computationally obtained peptide-

dx.doi.org/10.1021/ci400477e | J. Chem. Inf. Model. 2013, 53, 3280−3296

Table 1. Summary of Properties of AMP Sequences with Known IC_{50}[49,68]

	IC_{50}	MAX	MIN	MID	integration	E^b	H^c	length	scenario
V7K	0.03	8.55	−4.61	3.19	−0.70	6	0.24	12	2
A3R[a]	0.03	3.67	−4.84	−9.28	−11.7	6	0.39	12	1
A11C	0.04	5.38	−4.64	−0.45	−0.92	5	0.98	12	1
sub3[a]	0.04	7.77	−5.37	0.17	−2.01	7	−0.53	12	2
sub5	0.04	5.14	−12.22	−12.22	−23.78	7	−0.90	12	1
A3W	0.04	9.96	−4.77	1.06	0.21	5	0.69	12	2
V7Q	0.05	6.57	−2.75	1.78	4.17	5	0.28	12	2
sub2[a]	0.05	5.29	−3.53	−9.63	−13.18	7	−0.13	12	1
bac8c[a]	0.05	7.48	−9.09	1.28	−7.99	4	−0.26	8	2
I5W	0.06	5.46	−7.11	−0.1	−2.44	5	0.47	12	1
bac8a	0.06	2.14	−8.86	−1.52	−12.20	4	−0.19	8	1
bac8b	0.06	4.44	−8.30	1.02	−8.41	4	−0.26	8	2
A11Y	0.07	2.19	−5.57	−5.54	−8.56	5	0.66	12	1
A11H	0.08	4.34	−6.63	−0.35	−8.74	5	0.50	12	1
sub6	0.08	3.33	−14.49	−11.88	−32.13	5	−0.73	12	1
A11V	0.10	8.99	−4.04	1.96	1.74	5	1.12	12	2
A11S	0.10	6.26	−4.97	2.46	0.07	5	0.70	12	2
WT	0.13	7.12	−3.77	0.30	2.15	5	0.92	12	2
V10R[a]	0.18	13.76	−4.56	5.49	4.57	6	0.19	12	3
V7S	0.26	9.18	−2.34	5.83	8.57	5	0.50	12	3
R1Q	0.33	15.32	−4.01	11.2	9.92	4	1.00	12	3
bac8d[a]	0.39	12.51	−8.27	7.20	−1.81	5	−1.39	8	3
I8N	0.40	8.37	−3.96	7.37	5.32	5	0.25	12	3
R9V	0.49	12.51	−4.22	10.52	6.97	4	1.64	12	3
I8G	0.50	7.88	−3.03	3.61	5.59	5	0.51	12	2
R12W	0.75	9.18	−6.26	4.53	−0.20	4	1.22	12	2
V10E	0.75	8.37	−3.42	4.89	6.52	4	0.28	12	2
R12C	0.75	6.70	−4.12	3.94	3.36	4	1.50	12	2

[a]Simulation data from C-terminal penetration data. [b]E represented the net charge of the AMP sequences. [c]H represented the mean values of hydrophobicity, which were represented as Grand Average Hydrophobicity Value (GRAVY), calculated as the sum of hydropathy values of all the amino acids, divided by the number of residues in the sequence. Positive value of the score indicates hydrophobic and negative score indicates hydrophilic peptide.[69] Notation for mutated sequences is represented by a "letter-number-letter" code, where the first letter is an original residue name in wild type, the number is the corresponding residue position in wild type to be mutated, and the last letter is the mutated residue name.

membrane interactions (PMF). Additionally, to rigorously validate our simulation models, we also tested four double-substitution mutants and four octapeptides derived from the dodecapeptides for comparison. Thus, including wild type sequence, a total of 28 of these sequences were selected by their IC_{50} values for testing the discrimination accuracy of MD simulations. Among the 28 sequences, 17 sequences (10 single substitutions, four double substitutions, and three octapeptides) had lower IC_{50} values than wild type (IC_{50} < 0.13), seven sequences (six single substitutions and one octapeptide) had slightly higher IC_{50} values than wild type (0.13 < IC_{50} < 0.5), and three sequences (three single substitutions) had much higher IC_{50} values than wild type (IC_{50} > 0.5). As shown in Figure 1, for each sequence, we have also considered two distinct insertion pathways of the peptide by pulling either C- or N-terminal into the lipid bilayer separately, yielding two different PMF curves. PMF profiles were calculated by sampling peptide−lipid interactions as a function of distance between the mass center of the peptide and the center of the lipid bilayer using the adaptive biasing force (ABF) method. Properties of these simulated AMPs are summarized in Table 1.

To validate our model systems and simulation protocols, we selected three sequences of WT (IC_{50} = 0.13), A11C (IC_{50} = 0.04), and R12C (IC_{50} = 0.75) to study their penetration processes across the bilayer. For each sequence, three different external forces of 900, 1000, and 1100 kJ/(mol nm^2) were applied to the N/C terminus of the peptide for facilitating its penetration. In Figure S1, for each peptide three independent MD simulations showed similar PMF profiles with very minor differences, indicating that the effect of external forces on peptide penetration is not significant. Only slight differences of three PMF profiles occurred at the bilayer interface and the bilayer interior (z < 1.0 nm), which could be due to the local interplay between the external driving forces and the elastic deformation of the bilayer. Unless stated otherwise, we performed all PMF-MD simulations at an intermediate external force of 1000 kJ/(mol nm^2).

To further test the reliability of the MARTINI force field, in Figure S2, we presented and compared the PMF profiles for the transfer of Bac2A peptide across a POPE/POPG(3:1) bilayer using both a MARTINI CG force field and a united-atom GROMACS (ffgmx) force field.[50] The effects of peptide insertion orientation on the PMF profiles were also examined using both force fields. It can be seen in Figure S2 that, regardless of different insertion pathways via either N-terminus or C-terminus orientation, PMF profiles obtained by the MARTINI force field were largely in good agreement with the corresponding PMF profiles obtained by the united-atom GROMACS force field, but the MARTINI force field produced more smooth PMF profiles than the GROMACS force field, probably due to the reduced frictional force in the MARTINI-CG model.

dx.doi.org/10.1021/ci400477e | J. Chem. Inf. Model. 2013, 53, 3280−3296

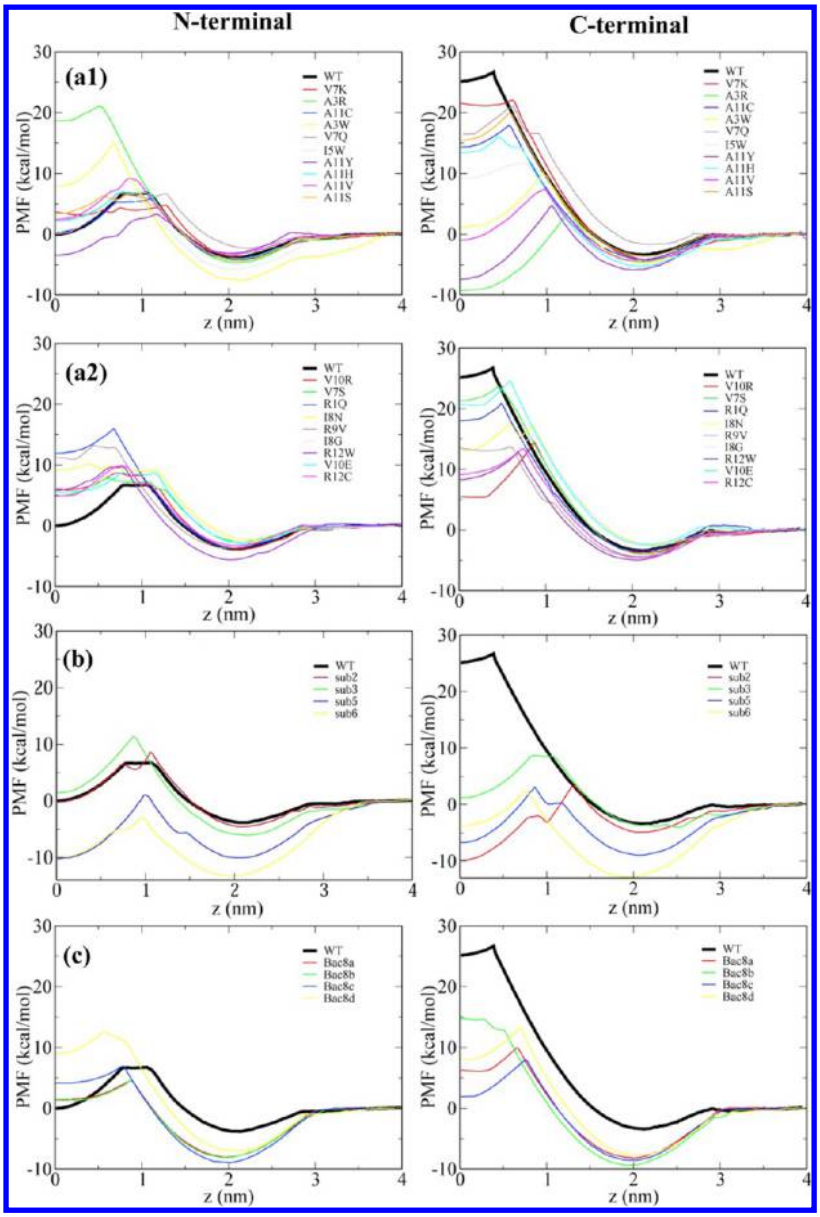

Figure 2. PMF profiles for transfer of selected AMPs with identified IC_{50} across the POPE/POPG bilayer from bulk water phase, including (a1, a2) single substitution dodecapeptides, (b) multiple substitution dodecapeptides, and (c) multiple substitution octapeptides.

On the other hand, the insertion of Bac2A into the bilayer via different orientations indeed yielded different PMF profiles. As Bac2A started to approach the lipid bilayer via the N-terminus (Figure S2a), it showed a favorable affinity to the bilayer surface with an energy well of −3.8 kcal/mol at 2 nm (compared with bulk water phase of $z \geq 4$ nm), but penetration of the peptide into the bilayer interior of ∼1 nm was hindered by a modest energy barrier (7.1 kcal/mol), followed by a further decreased energy barrier along the penetration pathway toward the center of the bilayer. In contrast, with the C-terminal insertion, Bac2A exhibited similar small affinity (−3.2 kcal/mol) to the bilayer surface but encountered a significant resistance at the entry and further penetration (Figure S2b). Comparison of PMF profiles with different insertion pathways suggests that Bac2A prefers to bind to the water/lipid interface, but the translocation of this peptide into the bilayer interior is much less energetically favorable and encounters a greater barrier. This phenomenon becomes even more pronounced for peptide insertion via the C-terminus, suggesting that N-terminal insertion of Bac2A is more energetically favorable, if such membrane insertion does occur. It should be noted that despite the convergence of the herein calculated PMF profiles, the free energy profile is still very difficult to estimate accurately along a simple reaction coordinate (i.e., distance between the mass center of the peptide and the center of the bilayer). Apart from vertical insertion (90°) of N-/C-termini of the wild type into the lipid bilayer, we also examined three different orientational insertion modes of wild type into POPE/POPG bilayers, e.g., wild type inserts into the bilayer via a parallel orientation to lipid surface, and tilted N-/C-terminal insertions of 45° relative to a bilayer normal (Figure S3). The parallel orientational insertion of WT led to a higher energy barrier than other insertion modes. A comparison of PMF curves between vertical terminal insertions and its corresponding tilted insertions showed similar insertion patterns, but tilted insertions always have the higher energy barriers than vertical insertions. These results are not surprising,

dx.doi.org/10.1021/ci400477e | J. Chem. Inf. Model. 2013, 53, 3280−3296

because tilted insertions of the peptide generally encounter relatively larger steric resistance with lipids. We should also note that different tilted insertions could provide the possibilities for transport of other peptides with the lower PMF pathways, but here we decided to use only the N-/C-terminal insertion in the rest of the simulations to make the computational approach simple and efficient.

3.2. PMFs of Antimicrobial Dodecapeptides with Single Substitutions. We computationally studied 19 single-point mutants from Hilpert's work to investigate the complete penetration process of the mutants toward the center of a mixed POPE/POPG (zwitterionic/anionic) lipid bilayer as model eukaryotic or prokaryotic cell membranes using the MARTINI CG-MD simulations. The distance-dependent PMF was calculated to determine the trans-membrane capability of the peptides, which will be used to correlate with or complement experimental IC_{50} values. As shown in Figure 2, by varying the mutated sequences of Bac2A and different insertion orientations, different mutants crossed the lipid bilayer differently. To better quantify the transmembrane activity, for a given N- or C-terminal insertion, we classified the mutants into two groups based on their IC_{50}: active mutants (IC_{50} < 0.13, Figure 2a1) and inactive mutants (IC_{50} > 0.13, Figure 2a2). In Figure 2a1, when 10 active mutants inserted into the lipid bilayer via the N-terminus, the mutants displayed a favorable energy well of −7.1 to −2.8 kcal/mol at the water/lipid interface (∼2 nm) similar to the wild type. However, as the mutants further penetrated into the lipid bilayer (z = 0.5−1.0 nm), 8 out of 10 active mutants (except A11H and A3W) displayed relatively small energy barriers of 2.2−8.6 kcal/mol, while A11H and A3W displayed larger energy barriers of 15.2−21.8 kcal/mol. When the mutants were inserted into the lipid bilayer via the C-terminus, the mutants also favored being adsorbed at the bilayer interface. Although all of the active mutants had relatively lower energy barriers than the wild type, six mutants still suffered from high energy barriers (>12 kcal/mol), which prevented them from membrane insertion, while the remaining four mutants (including A11H and A3W) displayed relatively small energy barriers of 3.5−9.9 kcal/mol at z = 0.5−1.0 nm. Thus, taking the PMFs together, all active mutants, either by N-/C-terminal insertion or both displayed −7.1 to −2.8 kcal/mol at the water/lipid interface and 2.2−9.9 kcal/mol at z = 0.5−1.0 nm. As these barriers were crossed, however, the translocation of active mutants toward the bilayer center seems to be favored (−9.3−3.2 kcal/mol at z = 0 nm).

In Figure 2a2, when all nine inactive mutants inserted into the lipid bilayer via either the N-terminus or C-terminus, the mutants displayed a favorable energy well of −6.3 to −2.3 kcal/mol at the water/lipid interface (∼2 nm) similar to wild type and active mutants. However, as the mutants further penetrated into the lipid bilayer (z = 0.5−1.0 nm), the inactive mutants encountered the higher energy barriers of 6.7−15.3 kcal/mol. Moreover, being different from the active mutants, even these barriers were crossed, however, the translocation of the inactive mutants toward the bilayer center seems to be forbidden due to the high energy barriers of 5.5 to 11.2 kcal/mol at z = 0. Taken together, a comparison of all PMF profiles of the mutants with different insertion pathways reveals several important findings: (1) Most mutants display a preferential orientation (N-terminus or C-terminus) for membrane insertion. (2) All mutants tend to adsorb on the lipid surface similar to the wild type. (3) Only active mutants display strong translocation ability across the membrane. If penetration occurs (in the case of 10 active mutants), two mutants prefer to penetrate into the bilayer via the C-terminus, six mutants via the N-terminus, and two mutants via either the C-terminus or N-terminus, indicating a close relationship between predicted trans-membrane ability and IC_{50}. (4) Even single substitution can alter the energy landscape for peptide penetration into the lipid membrane, resulting in the change of antimicrobial activity.

3.3. PMFs of Antimicrobial Dodecapeptides with Multiple Substitutions. Many studies have shown that positively charged residues (Lys and Arg) and hydrophobic aromatic residues (Trp and Phe) play an important role in modulating the membrane penetration process through electrostatic and/or hydrophobic interactions. Herein, we further selected four mutants (sub2 = RLRRIVVIRVRR, sub3 = RRWRIVVIRVRR, sub5 = RRWKIVVIRWRR, and sub6 = RWWKIWVIRWWR) with multiple-site mutations by Lys, Arg, and/or Trp for examining how these positively charged and hydrophobic aromatic residue substitutions affect the trans-membrane activity and associated energy landscapes. Experimentally, these four mutants have demonstrated their improved activities (IC_{50} = 0.04−0.08) as compared with Bac2A (IC_{50} = 0.13). Consistently, PMF profiles (Figure 2b) showed that for both N- and C-terminal insertion, three mutants (sub2, sub5, and sub6) displayed lower energy wells at the lipid interface and lower energy barriers at 1 nm than the wild type, suggesting that these three mutants improve their membrane adsorption and membrane insertion capacity compared with the wild type. Additionally, when inserting all mutants via the C-terminus, energy barriers were greatly reduced by up to 18 kcal/mol. Substitutions of Lys and Arg in multiple sites of Bac2A appear to facilitate electrostatic interaction between the positively charged side chains and the negatively charged phosphate groups of the bilayer, promoting the initial anchoring and adsorption of the peptide on the bilayer surface. Trp substitutions could interact strongly with hydrophobic tails of lipids for further membrane insertion. Additionally, Trp substitutions can also enhance peptide aggregation in solution and on the bilayer surface via $\pi-\pi$ interactions, which facilitate a conformational change of peptides and increase surface concentration of the peptides for membrane disruption. As compared with single substitution, the transmembrane activity of the mutants by multiple substitutions was improved or equivalent to (sub3) the wild type.

3.4. PMFs of Shorter Antimicrobial Octapeptides. The shorter AMPs are less expensive and thus more broadly studied. Herein, we truncated Bac2A at 4−11 positions to obtain an octapeptide (i.e., fragment of $Bac2A_{4-11}$), which was further mutated by Lys, Arg, and/or Trp at different positions to obtain four octapeptides (Bac8a = KIWVIRWR, Bac8b = RIWVIRWR, Bac8c = RIWVIWRR, and Bac8d = RRWVIWRR). Experimentally, as compared to the wild type (IC_{50} = 0.13), three mutants (Bac8a, Bac8b, and Bac8c) had shown improved activities (IC_{50} = 0.05−0.06), while one mutant (Bac8d) displayed poor activities (IC_{50} = 0.39). PMF profiles (Figure 2c) showed that three mutants (Bac8a, Bac8b, and Bac8c) displayed a relatively lower energy well at the lipid interface regardless of N-/C-terminus insertion. Energy barriers of all mutants remained at a similar level to that of the wild type for N-terminal insertion but were greatly reduced for C-terminal insertion. In line with single/double-substitution results, octapeptide and multiple-substitution dodecapeptides had a similar energy well (−9.1 to −7.1/−14.5 to −3.5 kcal/mol) at

dx.doi.org/10.1021/ci400477e | J. Chem. Inf. Model. 2013, 53, 3280−3296

the water/lipid interface (~2 nm), which was lower than single-substitution dodecapeptides (−7.1 to −2.8 kcal/mol). This suggests that the appropriate design of multiple-substitution mutants with different sequence lengths will effectively improve their membrane binding/penetrating activities than single-substitution mutants.

3.5. Correlation between Computational Transmembrane Ability and Experimental Antimicrobial Activity. All of the PMF curves we tested for a total of 28 sequences displayed similar horizon "S-like" shape (Figure 2), with three unique values: a minimum value (MIN) at z = ~2.0 nm (i.e., at the water/bilayer interface), a maximum value (MAX) at z = ~1.0 nm (i.e., at the half depth of a top leaflet), and a middle value (MID) at z = 0 nm (i.e., at the center of the lipid bilayer). The area under the PMF curve was also integrated from z = 0 nm to z = 4 nm to represent a total energy dissipation upon membrane insertion. The MIN value of <0 (compared to the water phase) presents a favorable location for peptides to be adsorbed at the water/bilayer interface, where nonspecific electrostatic interactions between positively charged peptides and anionic lipids could facilitate initial membrane adsorption. MIN values of all AMPs were smaller than 0, and the average MIN value was −6.1 kcal/mol, indicating that all 28 sequences bearing a net charge of >+1e displayed certain binding affinity to the negatively charged POPE/POPG (3:1) membrane. MAX values of all sequences were larger than 0 except sub6, indicating that a common energy barrier exists for peptide penetration. It should be noted that the bilayer interior is a less preferred location for the peptide to stay but should not be fully excluded, particularly when the transmembrane energy barrier (MAX value) is not too high and the MID value is close to or less than 0. This implies that once the energy barrier is crossed, further penetration of the peptide toward the center of the bilayer will follow a downhill pathway with the least resistance of free energy. MID and integration values showed a wide range of free energy landscapes from −12.2 to 11.2 kcal/mol and from −32.1 to 9.9 kcal/mol, respectively.

Based on the MAX, MIN, and MID values in the PMF profiles (Figure 2 and Table 1), different membrane insertion scenarios and different preferred peptide locations can be identified by mapping out peptide-lipid energy landscapes along peptide insertion pathways: (1) when MIN < 0 kcal/mol, MAX < 12 kcal/mol, and MID < 0 kcal/mol, nine mutants seem to have two favorable positions in the lipid bilayer: one at the bilayer surface with dominant propensity and the other inside the hydrophobic core of the lipid bilayer with minor propensity; (2) when MIN < 0 kcal/mol, MAX < 12 kcal/mol, and 0 < MID < 5 kcal/mol, 13 mutants prefer to stay at the water/bilayer interface or partially insert into the transmembrane position, similar to the first scenario; (3) when MIN < 0 kcal/mol, MAX> 12 kcal/mol or MIN < 0 kcal/mol, and MID> 5 kcal/mol, six mutants only show strong preference to stay at the water/bilayer interface—it is very unlikely for peptides to cross a high transmembrane energy barrier for membrane insertion; and (4) when MIN > 0 kcal/mol, mutants should prefer to stay in the water phase, and in our work, no mutants had MIN > 0 kcal/mol due to strong electrostatic interactions. We classified 28 sequences into these four membrane-insertion scenarios in Table 1.

To quantitatively correlate the MIN, MAX, MID, and integration values with the IC_{50} values for all 28 sequences, four stepwise regression models were used to analyze the importance and relevance between four PMF values and IC_{50}. Using multiple regression models also helps to improve the robustness of the analysis. As shown in Figure 3, using IC_{50} = 0.35 as a threshold value, four regression models enabled the separation of all data sets into a cluster region (IC_{50} < 0.35) and a scattered region (IC_{50} > 0.35), as fitted by two linear relationships, respectively. The cluster data showed a visible correlation for all four models. The best data fitting was observed for the MAX-IC_{50} correlation (R_1^2 = 0.52), suggesting that the transmembrane energy barrier is critical for antimicrobial activity. The MIN-IC_{50} data showed the weakest correlation (R_1^2 = 0.17), probably because most of peptides

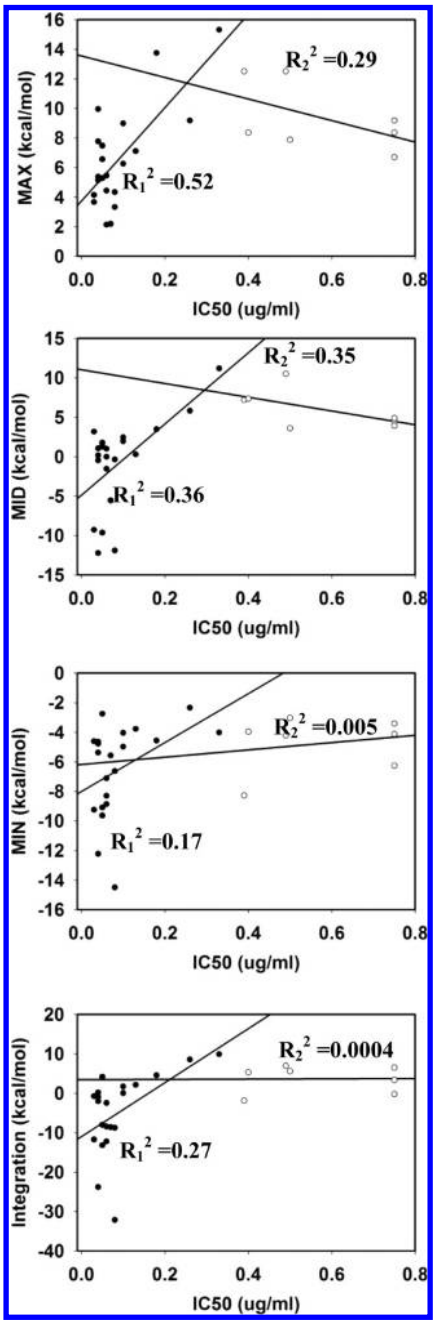

Figure 3. Regression analysis of the correlation between the MAX, MID, MIN, and integration-area values of the PMFs (transmembrane ability) and IC_{50} values (antimicrobial activity) for selected AMPs. Filled circles represent the AMPs with IC_{50} < 0.35, while the open circles represent the AMPs with IC_{50} > 0.35.

dx.doi.org/10.1021/ci400477e | J. Chem. Inf. Model. 2013, 53, 3280−3296

Table 2. Favorable Single Amino Acid Substation at Different Positions of Bac2A (Optimized from ref 49)

	sequences											
	1	2	3	4	5	6	7	8	9	10	11	12
	R	L	A	R	I	V	V	I	R	V	A	R
hydrophobic	W	W	W		W	W				W		
		C	C		C	C	C	C	C	C	C	
			I				I				I	
			F			F						
			L								L	
											M	
charged		R	R		R		R				R	
		K	K				K				K	
polar			Q				Q					
		S									S	
		G									G	
							N					
							T					
		Y									Y	
		H	H				H				H	

tested in this study displayed membrane binding ability, almost independent of their sequences. R_1^2 values were 0.36 for the MID-IC_{50} data and 0.27 for the Integration-IC_{50} data, respectively. However, we should point out that the scatter data in the plots indicate that transmembrane ability is likely not the sole determinant of antimicrobial activity. Consider that concentration-dependent membrane disruption mechanisms (i.e., pore-forming models and carpet model), as well as the complex nature of erythrocyte cell membranes containing glycoproteins and glycolipids, are not considered by our PMF-MD simulations. Moreover, in this study, only a single peptide was considered for membrane insertion, while multiple copies of the peptides across the lipid bilayers were not simulated to study the concentration effects on membrane deformations via membrane fusion or pore formation. If multiple peptides are involved in membrane penetration, the energy barrier for membrane insertion is likely to be reduced because the peptides are likely aggregate and adsorb at the membrane surface to enhance their interactions with the membrane. But, the PMF profile of a single peptide upon membrane penetration could still serve as a good indicator to discriminate the membrane insertion ability of the peptides.

3.6. Design of AMPs with Double Substitutions. On the basis of the discrimination ability of IC_{50} as reported by Hilpert et al.[49] and our PMF data, we summarized the favorable amino acid substitutions at various sites in Table 2. It can be seen clearly that (1) Arg, Trp, and Cys substitutions are often preferred to the original residues and (2) some positions of 2, 3, 7, and 11 are particularly rich for substitutions, while the other positions of 4, 8, 9, 10, and 12 have no or less preference for substitutions. Considering that a complete mutation test requires $20^{12} = \sim 4.1 \times 10^{15}$ sequences, which is an infeasible task to be examined by the PMF-MD simulations. Here, based on Table 2, we selected two important and representative residues of Arg and Trp to guide our design of new AMPs with double substitutions by Arg, Trp, or combined. We first designed a total of 40 double-substitution mutants at different favorable sites including 10 R/R, 15 W/W, and 15 R/W (Table S1). We then examined the transmembrane activity of these designed mutants using the PMF-MD simulations (Figure 4). With W/W mutations, regardless of insertion orientation, all W/W mutants displayed similar PMF profiles with pronounced minima (−10.9 to −4.8 kcal/mol, compared to the water phase) at the bilayer surface (∼2 nm) as compared with Bac2A, suggesting that all W/W mutants have strong preference staying at the bilayer surface. Thirteen out of 15 W/W mutants displayed relatively low or moderate energy barriers (3.1 to 8.9 kcal/mol) inside the bilayer of ∼1 nm. This implies that there also exists a certain possibility for W/W mutants to partially insert into the bilayer, although the center of the bilayer was a less preferred location, but not fully excluded due to relatively small transmembrane barriers. All R/R mutants featured small minima at the interfacial position (∼−3.8 to −0.9 kcal/mol) similar to Bac2A, but most of them encountered large transmembrane energy barriers (9.1 to 17.2 kcal/mol) for membrane insertion except for 2R11R, 3R11R, and 7R11R. Mixed R/W mutants behaved in between R/R and W/W mutants. All 15 R/W mutants showed lower energy minima in PMF profiles than Bac2A, and this indicates that all R/W mutants had strong preference for the water/bilayer position. Nine out of 15 W/W mutants displayed relatively low or moderate energy barriers (5.2 to 11.1 kcal/mol) inside the bilayer of ∼1 nm. Meanwhile, all R/W mutants disfavored penetrate into the bilayer via N-terminal, instead of C-terminal compared with Bac2A. Besides the favorable double mutations of WW/RR/RW, we also designed a 9E10E mutation as a negative control. As expected, the presence of two anionic Glu residues resulted in strong repulsive interactions with an anionic bilayer, showing much higher values of MIN/MAX/MIN values than the wild type (Figure 4d) and thus indicating a poor membrane penetrating ability.

Besides the W/W, R/R, and R/W double mutations, we also selectively examined the effect of double mutations of other hydrophobic (H), polar (P), and charge (C) residues on the transmembrane activity and associated energy landscapes using the PMF-MD simulations. A total of 10 000 new double-mutation sequences were generated using the mutation table (Table 2). Then, we applied an online support vector machine (SVM) tool in the database of CAMP (Collection of Anti-Microbial Peptides)[46] to select 17 sequences with high potency antimicrobial activity of ≥ 0.98 and four sequences with low potency antimicrobial activity of <0.6. This SVM uses a polynomial kernel function to quantitatively predict the possibility of any peptide to be a nonantimicrobial peptide or

dx.doi.org/10.1021/ci400477e | J. Chem. Inf. Model. 2013, 53, 3280−3296

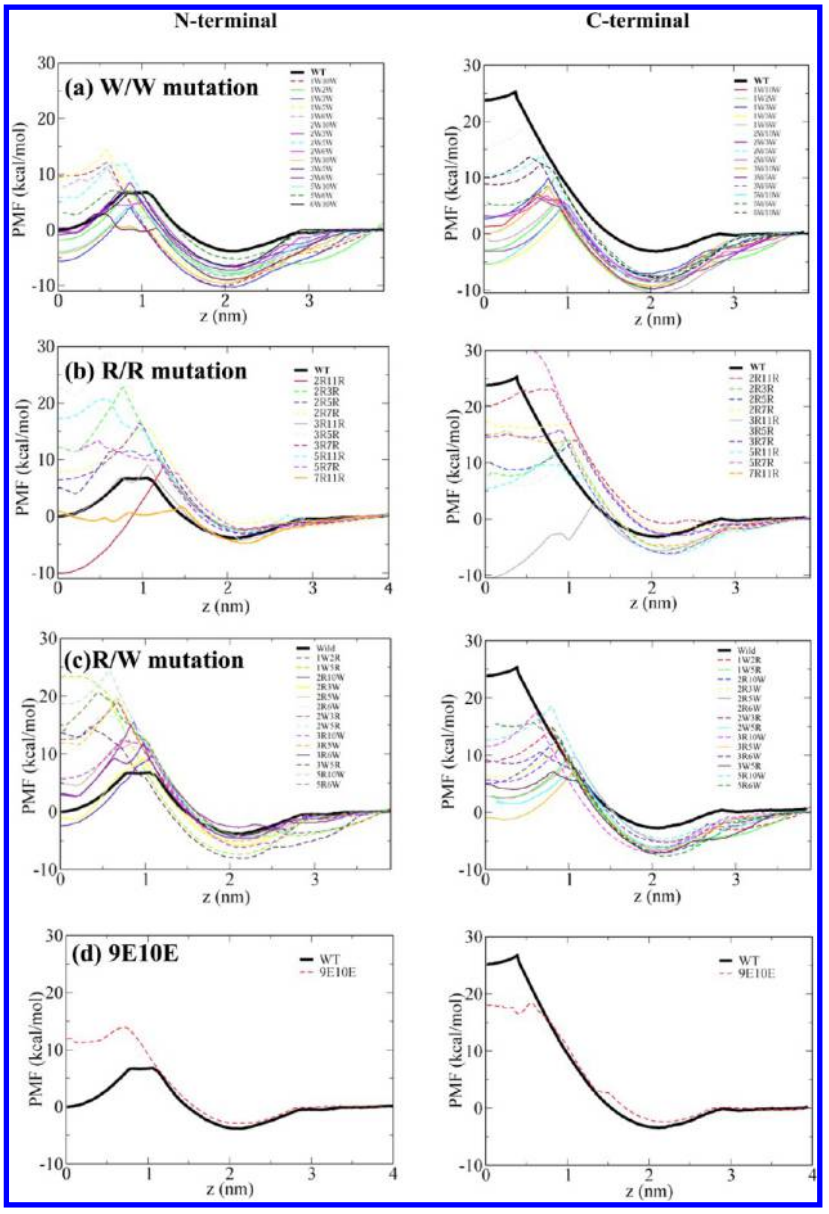

Figure 4. PMF profiles for transfer of the designed double-substitution mutants (W/W, R/R, R/W, and E/E) of Bac2A across the POPE/POPG bilayer from bulk water phase. Mutants presented by solid lines (dash lines) have a relatively strong (weak) trans-membrane ability compared with the wild type.

an antimicrobial peptide in the range of 0 (most impossible) to 1 (most possible). A total of 21 sequences were classified into three categories: 10 H/H, six H/C, and five P/X double-substitution mutants, where X represented H, C, or P (Table S2 and Figure 5). Eight of 10 H/H mutation sequences showed strong membrane penetration potential (Figure 5a, solid line), as indicated by the smaller MIN (−8.9 to −3.0 kcal/mol), MAX (−3.7 to 6.0 kcal/mol), and MID (−12.8 to 1.9 kcal/mol) values. The results were consistent with the W/W mutations, suggesting that hydrophobic substitutions can improve the antimicrobial activity of Bac2A. H/C mutation showed similar PMF trends to R/W mutation. Five out of six H/C mutants had lower energy minima than Bac2A, and three H/C mutants had lower or equivalent maxima to Bac2A (Figure 5b). With polar substitutions, all five P/X sequences showed higher or similar MAX/MID values compared with the wild type (Figure 5c). It seems that the introduction of polar residues hardly improves the membrane penetration ability.

It is generally accepted that hydrophobic aromatic and cationic residues are key residues that contribute to the antimicrobial activity of amphipathic AMPs. In our double-substitution designs, PMF profiles suggest that W/W mutations assist peptides for membrane adsorption and membrane insertion. Increased membrane association ability could be at least partially explained by the enhanced hydrophobic interactions with lipids and entropy effects for water repulsion around the hydrophobic residues. Surprisingly, the opposite behavior was observed for most Arg substitutions at various sites, showing weaker membrane association activity for most of the mutants. PMF data did not clearly reveal which position can promote or reduce membrane association activity. Arg substitution at the same position in different sequences often leads to different PMF patterns. Bac2A is an amphipathic peptide carrying a net charge of +4 and four Arg residues. Introduction of two additional Arg residues at various positions appears not to greatly promote membrane adsorption via

dx.doi.org/10.1021/ci400477e | J. Chem. Inf. Model. 2013, 53, 3280−3296

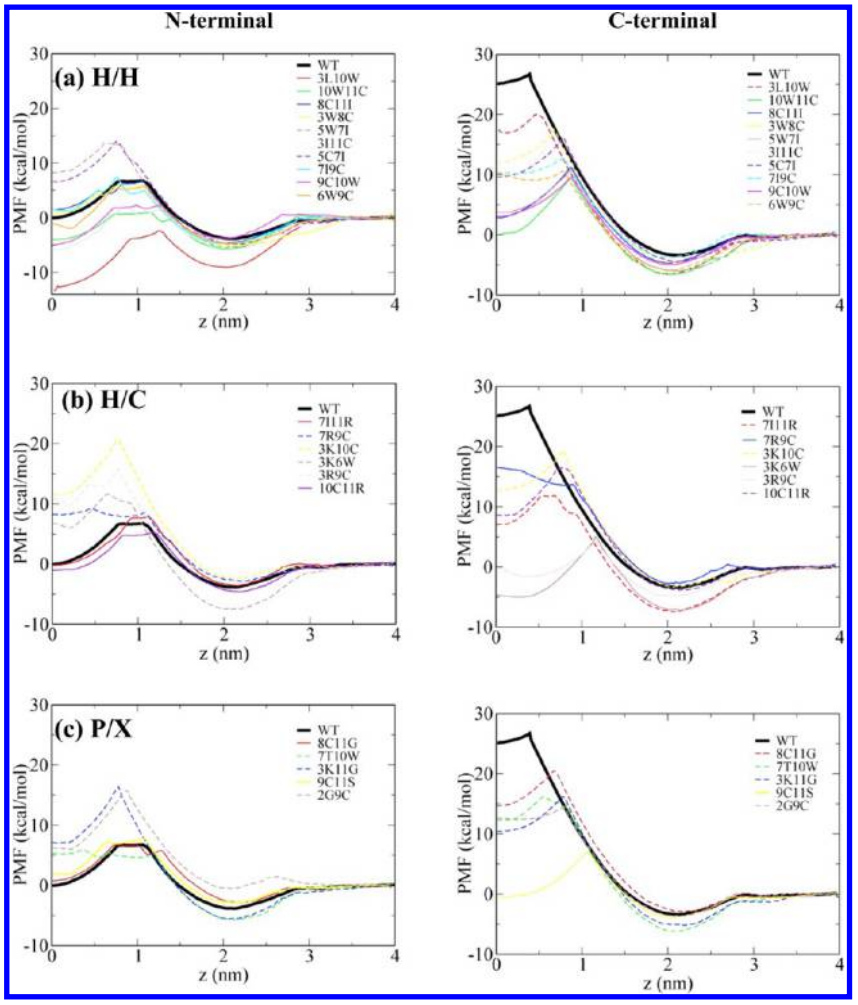

Figure 5. PMF profiles for the transfer of the designed double-substitution mutants (H/H, H/C, and P/X, where H = hydrophobic, P = polar, and C = charge residue) of Bac2A across the POPE/POPG bilayer from the bulk water phase. Mutants presented by solid lines (dash lines) have a relatively strong (weak) trans-membrane ability compared with the wild type.

electrostatic attraction between positively charged Arg residues and negatively charged phosphate groups in the POPE/POPG lipids. Instead, an imbalance of peptide composition between charge and hydrophobic residues would reduce hydrophobic interactions and thus prevent membrane penetration by the R/R mutants. Most of the mixed R/W and H/C mutants preferred to be adsorbed on the bilayer surface, similar to Bac2A. Taken together, based on the correlation between IC_{50} and PMF as described above, 40 of the 61 designed mutants were improved or equivalent to Bac2A (based on the PMF comparison), indicating that the mechanism of action of the AMPs can be readily modulated by some targeted double substitutions.

3.7. Screening of AMPs with Low Hemolytic Activity. Transmembrane ability of the AMPs plays a dual role in antimicrobial and hemolytic activity against both bacterial cells and human blood red cells, respectively. It is critical for improving the selectivity of designed AMPs with improved antibacterial activity against bacterial cells but reduced hemolytic activity for human red blood cells (hRBCs). The compositions of the bacterial membrane and hRBC membrane are dramatically different, where the former mainly contains anionic lipids while the latter consists of neutral lipids. Since melittin is well-known to induce the lysis of both bacterial and mammalian cells, it is used as a characteristic control to validate the PMF profiles against experimental observation. It can be seen clearly in Figure S4 that melittin adopted favorable transmembrane and interfacial locations from 0.5 to 2 nm (i.e., PMF $\leq$ 0 kcal/mol) in both lipid bilayers, suggesting strong cell selectivity of the mammalian cell membrane and thus strong toxicity and a hemolytic effect.

To obtain AMPs with high cell selectivity, we selected 14 dodecapeptides with IC_{50} values <0.13 from the Hilpert's data set (Figure 6) and 25 dodecapeptides with potential antibacterial activity from our PMF data (Figure 7) for probing their hemolytic activity. We performed CG-MD simulations to compare their PMF profiles across the neutral POPC bilayer (main component of hBRC membrane) with those across the anionic POPE/POPG (3:1) bilayer (main component of bacterial cell membrane). A total of 39 selected Bac2A variants and a wild type sequence have already demonstrated their antimicrobial activity computationally and experimentally, as described above. In Figure 7, regardless of the lipid bilayers, all PMF profiles displayed similar shapes with three distinct MIN, MAX, and MID values, so we used the previous PMF analysis based on MAX, MIN, and MID values to evaluate the transmembrane ability of the peptides across the POPC bilayer, which will be correlated with their hemolytic activities. Specifically, we identify the AMPs with high cell selectivity (i.e., strong transmembrane ability for POPE/POPG bilayer vs

dx.doi.org/10.1021/ci400477e | J. Chem. Inf. Model. 2013, 53, 3280−3296

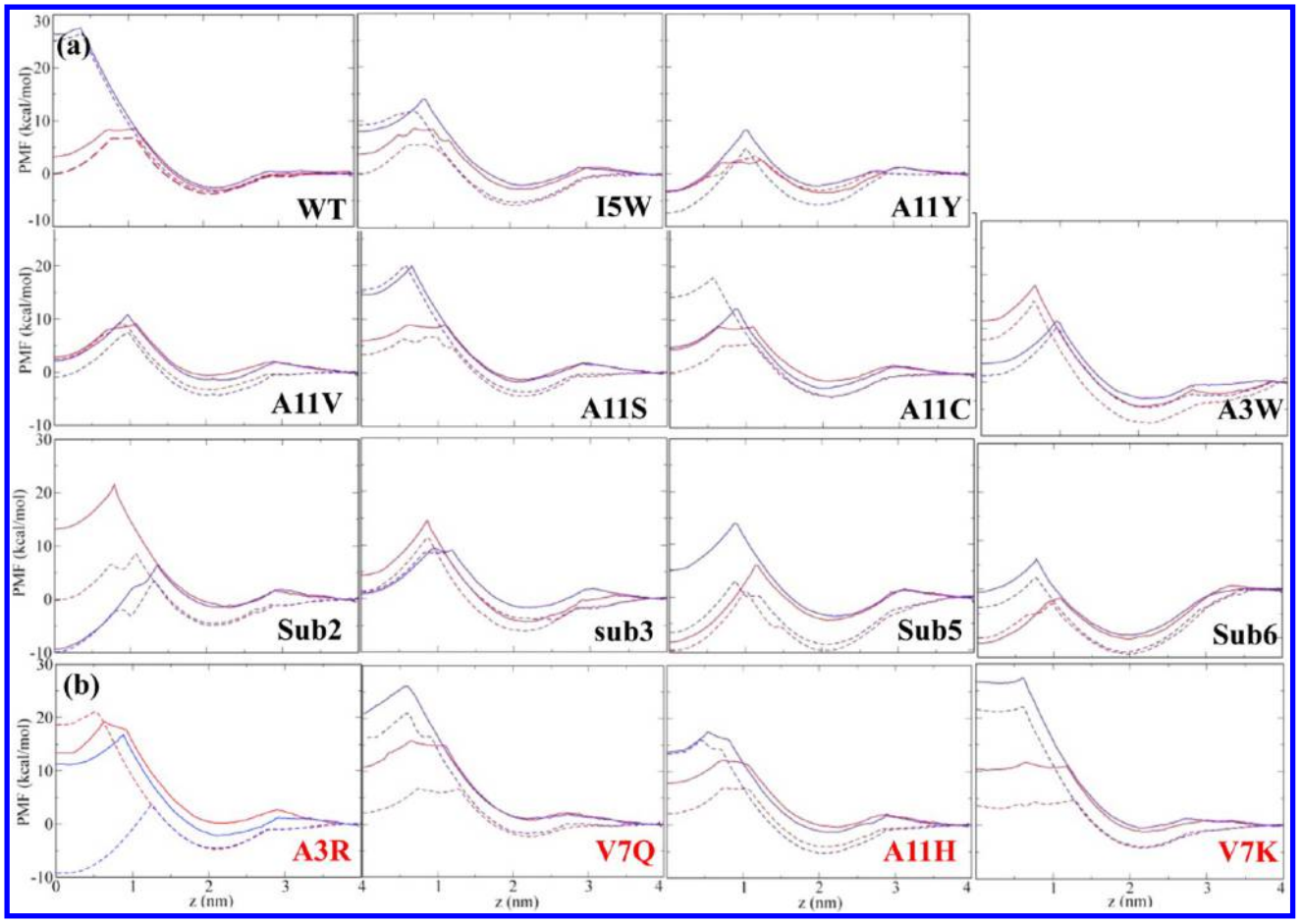

Figure 6. PMF profiles for transfer of 14 dodecapeptides with IC_{50} values <0.13 from Hilpert's data set across both the POPE/POPG bilayer (dash lines) and POPC bilayer (solid lines), resulting in (a) 10 mutants with poor cell selectivity and (b) four mutants with high cell selectivity. N-terminal (red color line) and C-terminal (blue color line) insertion pathways across both lipid bilayers are also presented for comparison.

weak transmembrane ability for POPC bilayer) using the following criteria: (i) Using a MAX value of 12 kcal/mol as a threshold, if the MAX values of POPC are >12 kcal/mol and the MAX values of POPE/POPG are <12 kcal/mol, this indicates that the peptide is more difficult to penetrate into POPC (low toxic to hBRC) than POPE/POPG (high toxic to bacterial cell), suggesting a high cell selectivity. (ii) If both POPC and POPE/POPG display lower MAX values of <12 kcal/mol and MID_{hRBC} > 5 kcal/mol (unfavorable penetration process for hRBC-mimic bilayer) and $\Delta(MID_{hRBC} - MID_{bacterial})$ > 5 kcal/mol (membrane discrimination ability), the peptide has a high cell selectivity. (iii) Otherwise, the peptide is identified as having poor selectivity in other situations.

With the criteria, among 14 mutants selected from Hilpert's data set, four mutants (A3R, A11H, V7Q, and V7K) displayed high cell selectivity. A3R, V7Q, and A11H encountered much higher resistance to penetration into the POPC bilayer than the POPE/POPG bilayer, as evidenced by great MAX values of >12 kcal/mol (Figure 6b). V7K displayed large membrane discrimination ability as evidenced by MID_{hRBC} > 5 kcal/mol and $\Delta(MID_{hRBC} - MID_{bacterial})$ > 5 kcal/mol, although V7K is likely to penetrate into both lipid bilayers (Figure 6b). The remaining 10 peptides and wild type showed similar PMF profiles as they traveled through both the POPE/POPG bilayer and POPC bilayer (Figure 6a). This indicates that the peptides have similar transmembrane abilities for both lipid bilayers and thus have similar antimicrobial and hemolytic activities (i.e., poor cell selectivity). Following a similar line, among 25 computationally designed mutants (Figure 7), five mutants (3W5W, 5W10W, 1W10W, 2W5R, and 7R11R) displayed good discrimination ability between POPC and POPE/POPG bilayers, while three mutants (2R6W, 3R6W, and 2R11R) likely lack the potential transmembrane ability to cross the POPC bilayer relative to the POPE/POPG (Figure 7b). This suggests that these eight peptides are likely to be potentially harmful to bacterial cells but not hBRCs because of their different membrane permeability. The other 17 mutants showed similar transmembrane ability to both POPE/POPG and POPC bilayers and thus cannot differentiate both bilayers effectively (Figure 7a). Moreover, comparison of the PMF profiles of the same peptide transporting through different lipid bilayers in Figures 6 and 7 revealed some interesting similarities for peptide transmembrane behaviors across different lipid bilayers. First, no matter how these peptides approach both bilayers via either the N-terminus or C-terminus, they all feature energy minima at the water/bilayer interface position (z = 2 nm) and present energy barriers at the bilayer interior (z = 1 nm) to prevent peptide penetration. This indicates that all peptides possess the membrane adsorption ability, which cannot be easily disturbed by substitutions. Additionally, consistent with previous results, all peptides showed a preferred insertion orientation, and the peptides take the least-resistant pathway via either N- or C-terminus for membrane insertion, depending on

dx.doi.org/10.1021/ci400477e | J. Chem. Inf. Model. 2013, 53, 3280−3296

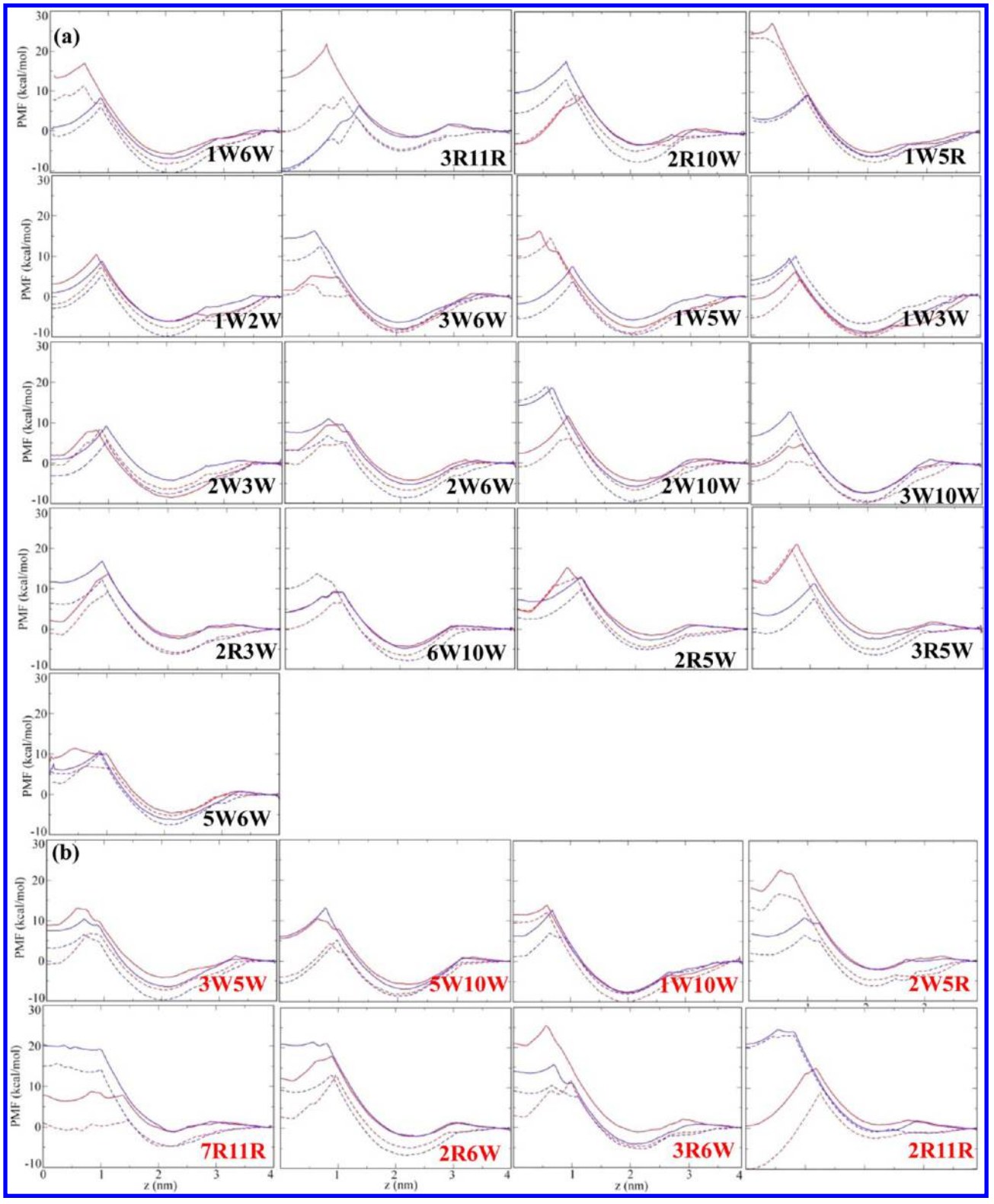

Figure 7. PMF profiles for transfer of 25 computationally designed dodecapeptides across both the POPE/POPG bilayer (dash lines) and POPC bilayer (solid lines), resulting in (a) 17 mutants with poor cell selectivity and (b) eight mutants with high cell selectivity. N-terminal (red color line) and C-terminal (blue color line) insertion pathways across both lipid bilayers are also presented for comparison.

peptide sequence/composition, lipid composition, and interplay peptide-lipid interactions.

3.8. Experimental Tests for Computationally Designed AMPs. To validate our design principles based on the PMF-IC_{50} relationship, we selected 10 peptides (two peptides from Hilpert's data set including wild type,[49] five peptides from designed double mutation sequences with a potential high therapeutic index, one peptide with low therapeutic index, and two peptides with no antibacterial activity as a negative control) for testing their antimicrobial and

hemolytic activities using a bacteria growth inhibition assay and hemolysis assay, as reported in Figure 8 and Table 3. Wild type

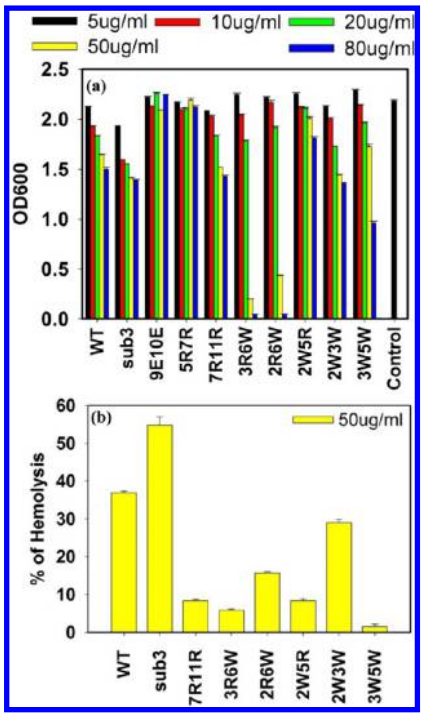

Figure 8. (a) Antimicrobial activities of selected AMPs at different peptide concentrations and (b) hemolytic activities of selected AMPs at 50 μg/mL.

and sub3 were used as positive controls, while 9E10E and 5R7R were used as negative controls. We first tested the antimicrobial activity of the peptides against *P. aeruginosa* under different peptide concentrations of 5, 10, 20, 50, and 80 μg/mL. As shown in Figure 8a, different peptides displayed different concentration-dependent antimicrobial activities, apparently reflecting the substitution effect. 9E10E and 5R7R peptides displayed poor antimicrobial activity, which was independent of peptide concentrations, as evidenced by an almost unchanged OD600 of 2.1 that was comparable to untreated bacterial cells. Consistent with the prediction by our double-substitution simulations described above, 9E10E and 5R7R peptides showed relatively high free energy resistance upon membrane insertion (Figure 4b and d). Substitution of neutral hydrophobic residues with two positively charged residues appears to imbalance the cooperative electrostatic and hydrophobic interactions, and compromise membrane activity and antimicrobial activity. Conversely, seven other peptides (sub3, 7R11R, 3R6W, 2R6W, 2W5R, 2W3W, and 3W5W) displayed enhanced antimicrobial activity as the concentration of the peptides increased. Among them, 3R6W and 2R6W with combined substitutions of positively charged residue of Lys and hydrophobic aromatic residue of Trp at a particular position 6 were the most active peptides against *P. aeruginosa* at 50 and 80 μg/mL. The sub3, 7R11R, 2W5R, 2W3W, and 3W5W showed modest antimicrobial activity to inhibit bacterial growth at the highest concentration of 80 μg/mL.

As a measure of biocompatibility, we further reported the hemolytic activity of the eight peptides (except 9E10E and 5R7R) to hRBCs using a fixed peptide concentration of 50 μg/mL. In Figure 8b, all eight peptides tested can be classified into three groups based on hemolysis (%): (1) 7R11R, 3R6W, 2W5R, and 3W5W exhibited a substantial low hemolytic activity of $\leq$10%; (2) WT, 2R6W, and 2W3W showed moderate hemolytic activity between 10% and 50%; and (3) sub3 had a severe hemolytic toxicity of ~55%. Comparison of antimicrobial and hemolytic results reveals that 3R6W and 2R6W with balanced substitution of charged and hydrophobic residues can be tuned to achieve the best antimicrobial activity while minimizing red blood cell lysis. 2W3W, 3W5W, and 7R11R containing either two aromatic Trp substitutions or two positively charged Arg substitutions show a general moderate activity for both bacterial cells and hRBCs. To better understand the membrane activity of these peptides, PMF data also confirm that 3R6W and 2R6W are more surface resistant to the neutral POPC bilayer than to the anionic POPE/POPG bilayer. The R/W substitutions suggest the enhanced affinity of the peptides to anionic lipids, but not neutral lipids, resulting in enhanced antimicrobial and reduced hemolytic activity. Additionally, because the MIC values often depend on the assay conditions and bacterial strains, and because many laboratories have developed their own protocols, it would be impractical to compare the MIC values for different compounds reported in the literature.

To better determine possible design principles, Figure 9 shows the mapping of the predicted cell selectivity (i.e., therapeutic index = $MID_{hRBC} - MID_{Bac}$) onto the two reaction

Table 3. Property Summary of Selected Dodecapeptides for Experimental Tests

sequences	name	IC_{50}	MID_{Bac}[a]	MID_{hRBC}[b]	index[c]	E[d]	H[e]
RLARIVVIRVAR-NH_2	WT	0.13	0.30	3.1	2.8	+5	0.92
RRWRIVVIRVRR-NH_2	sub3	0.04	0.17	1.25	1.08	+7	−0.53
RLARIVVIEEAR-NH_2	9E10E	N/A	11.72	N/A	N/A	+2	0.36
RLARRVRIRVAR-NH_2	5R7R	N/A	10.05	N/A	N/A	+7	−0.56
RLARIVRIRVRR-NH_2	7R11R	N/A	0.89	7.95	7.06	+7	−0.33
RLRRIWVIRVAR-NH_2	3R6W	N/A	2.65	13.70	11.05	+6	−0.03
RRARIWVIRVAR-NH_2	2R6W	N/A	2.72	12.30	9.58	+6	−0.20
RWARRVVIRVAR-NH_2	2W5R	N/A	1.7	7.32	5.62	+6	−0.23
RWWRIVVIRVAR-NH_2	2W3W	N/A	−3.10	1.3	4.4	+5	0.30
RLWRWVVIRVAR-NH_2	3W5W	N/A	−0.92	7.64	8.56	+5	0.24

[a]MID values from bacterial membrane penetration PMFs. [b]MID values from hRBC membrane penetration PMFs. [c]Therapeutic index = $MID_{hRBC} - MID_{Bac}$. [d]E represented the net charge of the AMP sequences. [e]H represented the mean values of hydrophobicity, which were represented as Grand Average Hydrophobicity Value (GRAVY), calculated as the sum of hydropathy values of all the amino acids, divided by the number of residues in the sequence. Positive value of the score indicates hydrophobic and negative score indicates hydrophilic peptide.[69]

dx.doi.org/10.1021/ci400477e | J. Chem. Inf. Model. 2013, 53, 3280−3296

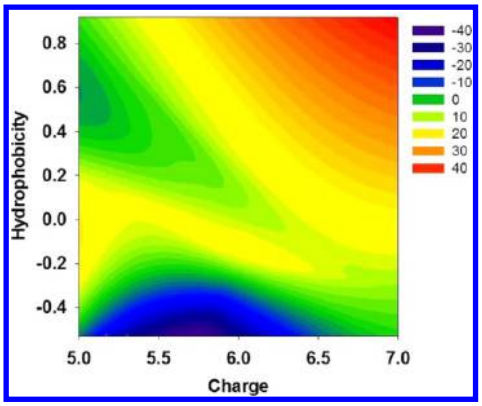

Figure 9. Mapping of the predicted cell selectivity (i.e., therapeutic index) of the AMPs onto the two reaction coordinates of hydrophobicity and net charge of the peptides.

coordinates of hydrophobicity and net charge of the eight peptides from Figure 8b. Cell selectivity from high to low values is presented by a red−green−blue color scale. Peptides located in the red region bear both high hydrophobicity and net charges, indicating that a simultaneous increase of hydrophobicity and charge characters together will improve the cell selectivity of designs. However, the sole increase of either hydrophobicity or charge achieves limited cell selectivity in the green region. Low hydrophobicity and low charge in the blue region should be avoided. From these results, we should also note that the membrane activity of the AMPs cannot be simply explained by a particular sequence or sequence motif, rather than more complex interplay among intrinsic physicochemical properties of peptides (i.e., size, composition, overall charge, hydrophobicity, secondary structure) and lipids (i.e., composition) and external conditions (peptide concentrations, assay conditions, and bacterial strains). The use of a coarse-grained MARTINI model to accurately describe the peptide-membrane interactions still remains a great challenge under intense development for better representing the structure and dynamics of water, peptides, and lipids. Actually, the potential structures and phenomena captured in the CG simulations can serve as a starting point and be refined in fully atomistic models and simulations. In addition, only single-peptide penetration was evaluated rather than synergistic multiple-peptide penetration. Even with these limitations, our PMF data obtained from the translocation of a single peptide across different lipid bilayers still can help to distinguish between different possible models of membrane adsorption and insertion.

4. CONCLUSIONS

In this work, we presented a comprehensive MD investigation of the membrane insertion of AMPs into anionic POPE/POPG and neutral POPC bilayers, which mimic the main components of bacterial and hRBC membranes. Specifically, we used a hybrid simulation method combining the coarse-grained MARTINI model, adaptive biasing force (ABF) method, and the umbrella sampling technique with MD simulations to probe a complete translocation process of Bac2A and its variants across different lipid bilayers. The potential of mean force (PMF) associated with the peptide translocation process was calculated to directly determine the free energy barrier required to transfer the peptides from the bulk water phase to the water-membrane interface to the bilayer interior. A number of computationally designed sequences were identified and predicted with enhanced membrane association ability to the bacterial cell membrane while retaining membrane resistance to the hRBC membrane, which are well correlated with antimicrobial and hemolytic activities, respectively. Further bacterial inhibition and hRBC assays confirm that the most active mutants (3R6W and 2R6W) can indeed kill bacteria efficiently while minimizing harm to human cells. The balanced substitution of charged residue (Arg) and hydrophobic residue (Trp) in Bac2A can be tuned to achieve the best antimicrobial activity while minimizing red blood cell lysis via the cooperative interactions. A comparison of computational PMF data with experimental cell assay results reveals a statistical correlation between the transmembrane activity of peptides across different lipid bilayers and antimicrobial and hemolytic activities with reasonable accuracy. This work provides a platform for screening and the design of new effective AMPs with good cell selectivity.

■ ASSOCIATED CONTENT

Supporting Information

Includes two tables and four figures. This material is available free of charge via the Internet at http://pubs.acs.org.

■ AUTHOR INFORMATION

Corresponding Author

*E-mail: zhengj@uakron.edu.

Notes

The authors declare no competing financial interest.

■ ACKNOWLEDGMENTS

J.Z. thanks the National Science Foundation (CAREER Award CBET-0952624 and CBET-1158447) for financial support. G.L. is thankful for financial support from Natural Science Foundation Project of Chongqing CSTC (cstc2012ggjhz10003).

■ REFERENCES

(1) Marcos, J. F.; Manzanares, P. Antimicrobial Peptides. In *Antimicrobial Polymers*; John Wiley & Sons, Inc.: New York, 2011; pp 195−225.

(2) Brown, E. D.; Wright, G. D. New targets and screening approaches in antimicrobial drug discovery. *Chem. Rev.* **2005**, *105*, 759−774.

(3) Wimley, W. C. Describing the mechanism of antimicrobial peptide action with the interfacial activity model. *ACS Chem. Biol.* **2010**, *5*, 905−917.

(4) Neu, H. C. The crisis in antibiotic-resistance. *Science* **1992**, *257*, 1064−1073.

(5) Finberg, R. W.; Moellering, R. C.; Tally, F. P.; Craig, W. A.; Pankey, G. A.; Dellinger, E. P.; West, M. A.; Joshi, M.; Linden, P. K.; Rolston, K. V.; Rotschafer, J. C.; Rybak, M. J. The importance of bactericidal drugs: Future directions in infectious disease. *Clin. Infect. Dis.* **2004**, *39*, 1314−1320.

(6) Lai, X.-Z.; Feng, Y.; Pollard, J.; Chin, J. N.; Rybak, M. J.; Bucki, R.; Epand, R. F.; Epand, R. M.; Savage, P. B. Ceragenins: cholic acid-based mimics of antimicrobial peptides. *Acc. Chem. Res.* **2008**, *41*, 1233−1240.

(7) Hong, M. Solid-state NMR studies of the structure, dynamics, and assembly of β-sheet membrane peptides and α-helical membrane proteins with antibiotic activities. *Acc. Chem. Res.* **2006**, *39*, 176−183.

(8) Fjell, C. D.; Hiss, J. A.; Hancock, R. E. W.; Schneider, G. Designing antimicrobial peptides: form follows function. *Nat. Rev. Drug Discovery* **2012**, *11*, 37−51.

(9) Hancock, R. E. W.; Sahl, H. G. Antimicrobial and host-defense peptides as new anti-infective therapeutic strategies. *Nat. Biotechnol.* **2006**, *24*, 1551−1557.
(10) Hancock, R. E. W.; Lehrer, R. Cationic peptides: a new source of antibiotics. *Trends Biotechnol.* **1998**, *16*, 82−88.
(11) Hale, J. D. F.; Hancock, R. E. W. Alternative mechanisms of action of cationic antimicrobial peptides on bacteria. *Expert Rev. Anti Infect. Ther.* **2007**, *5*, 951−959.
(12) Velkov, T.; Thompson, P. E.; Nation, R. L.; Li, J. Structure−Activity Relationships of Polymyxin Antibiotics. *J. Med. Chem.* **2009**, *53*, 1898−1916.
(13) Tew, G. N.; Scott, R. W.; Klein, M. L.; DeGrado, W. F. De Novo design of antimicrobial polymers, foldamers, and small Molecules: from discovery to practical applications. *Acc. Chem. Res.* **2009**, *43*, 30−39.
(14) Dhople, V.; Krukemeyer, A.; Ramamoorthy, A. The human beta-defensin-3, an antibacterial peptide with multiple biological functions. *Biochim. Biophys. Acta, Biomembr.* **2006**, *1758*, 1499−1512.
(15) Chen, F.-Y.; Lee, M.-T.; Huang, H. W. Evidence for membrane thinning effect as the mechanism for peptide-induced pore formation. *Biophys. J.* **2003**, *84*, 3751−3758.
(16) Brogden, K. A. Antimicrobial peptides: pore formers or metabolic inhibitors in bacteria? *Nat. Rev. Microbiol.* **2005**, *3*, 238−250.
(17) Ramamoorthy, A.; Thennarasu, S.; Lee, D.-K.; Tan, A.; Maloy, L. Solid-State NMR Investigation of the Membrane-Disrupting Mechanism of Antimicrobial Peptides MSI-78 and MSI-594 Derived from Magainin 2 and Melittin. *Biophys. J.* **2006**, *91*, 206−216.
(18) Bhattacharjya, S.; Ramamoorthy, A. Multifunctional host defense peptides: functional and mechanistic insights from NMR structures of potent antimicrobial peptides. *FEBS J.* **2009**, *276*, 6465−6473.
(19) Ramamoorthy, A.; Lee, D.-K.; Narasimhaswamy, T.; Nanga, R. P. R. Cholesterol reduces pardaxin's dynamics—a barrel-stave mechanism of membrane disruption investigated by solid-state NMR. *Biochim. Biophys. Acta, Biomembr.* **2010**, *1798*, 223−227.
(20) Hong, M.; Su, Y. Structure and dynamics of cationic membrane peptides and proteins: Insights from solid-state NMR. *Protein Sci.* **2011**, *20*, 641−655.
(21) Tang, M.; Waring, A. J.; Lehrer, R. L.; Hong, M. Effects of guanidinium-phosphate hydrogen bonding on the membrane-bound structure and activity of an arginine-rich membrane peptide from solid-state NMR spectroscopy. *Angew. Chem., Int. Ed.* **2008**, *47*, 3202−3205.
(22) Chen, X.; Chen, Z. SFG studies on interactions between antimicrobial peptides and supported lipid bilayers. *Biochim. Biophys. Acta, Biomembr.* **2006**, *1758*, 1257−1273.
(23) Avery, C. W.; Som, A.; Xu, Y.; Tew, G. N.; Chen, Z. Dependence of Antimicrobial Selectivity and Potency on Oligomer Structure Investigated Using Substrate Supported Lipid Bilayers and Sum Frequency Generation Vibrational Spectroscopy. *Anal. Chem.* **2009**, *81*, 8365−8372.
(24) Ladokhin, A. S.; Selsted, M. E.; White, S. H. CD spectra of indolicidin antimicrobial peptides suggest turns, not polyproline helix. *Biochemistry (Moscow)* **1999**, *38*, 12313−12319.
(25) Turner, J.; Cho, Y.; Dinh, N. N.; Waring, A. J.; Lehrer, R. I. Activities of LL-37, a cathelin-associated antimicrobial peptide of human neutrophils. *Antimicrob. Agents Chemother.* **1998**, *42*, 2206−2214.
(26) Johansson, J.; Gudmundsson, G. H.; Rottenberg, M. E.; Berndt, K. D.; Agerberth, B. Conformation-dependent antibacterial activity of the naturally occurring human peptide LL-37. *J. Biol. Chem.* **1998**, *273*, 3718−3724.
(27) Ladokhin, A. S.; Selsted, M. E.; White, S. H. Bilayer interactions of indolicidin, a small antimicrobial peptide rich in tryptophan, proline, and basic amino acids. *Biophys. J.* **1997**, *72*, 794−805.
(28) Wimley, W. C.; White, S. H. Experimentally determined hydrophobicity scale for proteins at membrane interfaces. *Nat. Struct. Biol.* **1996**, *3*, 842−848.
(29) White, S. H.; Wimley, W. C. Membrane protein folding and stability: Physical principles. *Annu. Rev. Biophys. Biomol. Struct.* **1999**, *28*, 319−365.
(30) Ladokhin, A. S.; White, S. H. Folding of amphipathic alpha-helices on membranes: Energetics of helix formation by melittin. *J. Mol. Biol.* **1999**, *285*, 1363−1369.
(31) Kyrychenko, A.; Rodnin, M. V.; Posokhov, Y. O.; Holt, A.; Pucci, B.; Killian, J. A.; Ladokhin, A. S. Thermodynamic measurements of bilayer insertion of a single transmembrane helix chaperoned by fluorinated surfactants. *J. Mol. Biol.* **2012**, *416*, 328−334.
(32) Marrink, S. J.; de Vries, A. H.; Tieleman, D. P. Lipids on the move: Simulations of membrane pores, domains, stalks and curves. *Biochim. Biophys. Acta, Biomembr.* **2009**, *1788*, 149−168.
(33) La Rocca, P.; Biggin, P. C.; Tieleman, D. P.; Sansom, M. S. P. Simulation studies of the interaction of antimicrobial peptides and lipid bilayers. *Biochim. Biophys. Acta, Biomembr.* **1999**, *1462*, 185−200.
(34) Matyus, E.; Kandt, C.; Tieleman, D. P. Computer simulation of antimicrobial peptides. *Curr. Med. Chem.* **2007**, *14*, 2789−2798.
(35) Illya, G.; Deserno, M. Coarse-Grained Simulation Studies of Peptide-Induced Pore Formation. *Biophys. J.* **2008**, *95*, 4163−4173.
(36) Irudayam, S. J.; Berkowitz, M. L. Binding and reorientation of melittin in a POPC bilayer: Computer simulations. *Biochim. Biophys. Acta, Biomembr.* **2012**, *1818*, 2975−2981.
(37) Chen, X.; Wang, J.; Kristalyn, C. B.; Chen, Z. Real-time structural investigation of a lipid bilayer during its interaction with melittin using sum frequency generation vibrational spectroscopy. *Biophys. J.* **2007**, *93*, 866−875.
(38) Hicks, R. P.; Bhonsle, J. B.; Venugopal, D.; Koser, B. W.; Magill, A. J. De novo design of selective antibiotic peptides by incorporation of unnatural amino acids. *J. Med. Chem.* **2007**, *50*, 3026−3036.
(39) Dathe, M.; Wieprecht, T.; Nikolenko, H.; Handel, L.; Maloy, W. L.; MacDonald, D. L.; Beyermann, M.; Bienert, M. Hydrophobicity, hydrophobic moment and angle subtended by charged residues modulate antibacterial and haemolytic activity of amphipathic helical peptides. *FEBS Lett.* **1997**, *403*, 208−212.
(40) Blondelle, S. E.; Houghten, R. A. Design of model amphipathic peptides having potent antimicrobial activities. *Biochemistry (Moscow)* **1992**, *31*, 12688−12694.
(41) Oren, Z.; Hong, J.; Shai, Y. A repertoire of novel antibacterial diastereomeric peptides with selective cytolytic activity. *J. Biol. Chem.* **1997**, *272*, 14643−14649.
(42) Shai, Y.; Oren, Z. Diastereomers of cytolysins, a novel class of potent antibacterial peptides. *J. Biol. Chem.* **1996**, *271*, 7305−7308.
(43) Oren, Z.; Shai, Y. Selective lysis of bacteria but not mammalian cells by diastereomers of melittin: structure−function study. *Biochemistry (Moscow)* **1997**, *36*, 1826−1835.
(44) Fjell, C. D.; Hancock, R. E. W.; Cherkasov, A. AMPer: a database and an automated discovery tool for antimicrobial peptides. *Bioinformatics* **2007**, *23*, 1148−1155.
(45) Wang, Z.; Wang, G. S. APD: the Antimicrobial Peptide Database. *Nucleic Acids Res.* **2004**, *32*, D590−D592.
(46) Thomas, S.; Karnik, S.; Barai, R. S.; Jayaraman, V. K.; Idicula-Thomas, S. CAMP: a useful resource for research on antimicrobial peptides. *Nucleic Acids Res.* **2010**, *38*, D774−D780.
(47) Romeo, D.; Skerlavaj, B.; Bolognesi, M.; Gennaro, R. Structure and bactericidal activity of an antibiotic dodecapeptide purified from bovine neutrophils. *J. Biol. Chem.* **1988**, *263*, 9573−9575.
(48) Wu, M. H.; Hancock, R. E. W. Improved derivatives of bactenecin, a cyclic dodecameric antimicrobial cationic peptide. *Antimicrob. Agents Chemother.* **1999**, *43*, 1274−1276.
(49) Hilpert, K.; Volkmer-Engert, R.; Walter, T.; Hancock, R. E. W. High-throughput generation of small antibacterial peptides with improved activity. *Nat. Biotechnol.* **2005**, *23*, 1008−1012.
(50) Hess, B.; Kutzner, C.; van der Spoel, D.; Lindahl, E. GROMACS 4: Algorithms for Highly Efficient, Load-Balanced, and Scalable Molecular Simulation. *J. Chem. Theory Comput.* **2008**, *4*, 435−447.
(51) Dowhan, W. Molecular basis for membrane phospholipid diversity: Why are there so many lipids? *Annu. Rev. Biochem.* **1997**, *66*, 199−232.

(52) Uran, S.; Larsen, A.; Jacobsen, P. B.; Skotland, T. Analysis of phospholipid species in human blood using normal-phase liquid chromatography coupled with electrospray ionization ion-trap tandem mass spectrometry. *J. Chromatogr. B: Anal. Technol. Biomed. Life Sci.* **2001**, *758*, 265−275.
(53) Zhao, J.; Luo, Y.; Jang, H.; Yu, X.; Wei, G.; Nussinov, R.; Zheng, J. Probing ion channel activity of human islet amyloid polypeptide (amylin). *Biochim. Biophys. Acta, Biomembr.* **2012**, *1818*, 3121−3130.
(54) Yu, X.; Wang, Q.; Pan, Q.; Zhou, F.; Zheng, J. Molecular interactions of Alzheimer amyloid-beta oligomers with neutral and negatively charged lipid bilayers. *Phys. Chem. Chem. Phys.* **2013**, *15*, 8878−8889.
(55) Jang, H.; Zheng, J.; Nussinov, R. Models of {beta}-amyloid ion-channels in the membrane suggest that channel formation in the bilayer is a dynamic process. *Biophys. J.* **2007**, *93*, 1938−1949.
(56) Yu, X.; Zheng, J. Cholesterol promotes the interaction of Alzheimer β-amyloid monomer with lipid bilayer. *J. Mol. Biol.* **2012**, *421*, 561−571.
(57) Nugent, T.; Jones, D. Transmembrane protein topology prediction using support vector machines. *BMC Bioinf.* **2009**, *10*, 159.
(58) Jones, D. T. Improving the accuracy of transmembrane protein topology prediction using evolutionary information. *Bioinformatics* **2007**, *23*, 538−544.
(59) Marrink, S. J.; de Vries, A. H.; Mark, A. E. Coarse grained model for semiquantitative lipid simulations. *J. Phys. Chem. B* **2004**, *108*, 750−760.
(60) Kumar, S.; Rosenberg, J. M.; Bouzida, D.; Swendsen, R. H.; Kollman, P. A. The weighted histogram analysis method for free-energy calculations on biomolecules. I. The method. *J. Comput. Chem.* **1992**, *13*, 1011−1021.
(61) Berendsen, H. J. C.; Postma, J. P. M.; Vangunsteren, W. F.; Dinola, A.; Haak, J. R. Molecular dynamics with coupling to an external bath. *J. Chem. Phys.* **1984**, *81*, 3684−3690.
(62) Hub, J. S.; de Groot, B. L.; van der Spoel, D. g_wham - A free weighted histogram analysis implementation including robust error and autocorrelation estimates. *J. Chem. Theory Comput.* **2010**, *6*, 3713−3720.
(63) Rzepiela, A. J.; Schäfer, L. V.; Goga, N.; Risselada, H. J.; De Vries, A. H.; Marrink, S. J. Reconstruction of atomistic details from coarse-grained structures. *J. Comput. Chem.* **2010**, *31*, 1333−1343.
(64) de Jong, D. H.; Singh, G.; Bennett, W. F. D.; Arnarez, C.; Wassenaar, T. A.; Schäfer, L. V.; Periole, X.; Tieleman, D. P.; Marrink, S. J. Improved Parameters for the Martini Coarse-Grained Protein Force Field. *J. Chem. Theory Comput.* **2012**, *9*, 687−697.
(65) Monticelli, L.; Kandasamy, S. K.; Periole, X.; Larson, R. G.; Tieleman, D. P.; Marrink, S.-J. The MARTINI coarse-grained force field: extension to proteins. *J. Chem. Theory Comput.* **2008**, *4*, 819−834.
(66) Lopez, C. A.; Rzepiela, A. J.; de Vries, A. H.; Dijkhuizen, L.; Huenenberger, P. H.; Marrink, S. J. Martini Coarse-Grained Force Field: Extension to Carbohydrates. *J. Chem. Theory Comput.* **2009**, *5*, 3195−3210.
(67) Marrink, S. J.; Risselada, H. J.; Yefimov, S.; Tieleman, D. P.; de Vries, A. H. The MARTINI force field: Coarse grained model for biomolecular simulations. *J. Phys. Chem. B* **2007**, *111*, 7812−7824.
(68) Wieczorek, M.; Jenssen, H.; Kindrachuk, J.; Scott, W. R. P.; Elliott, M.; Hilpert, K.; Cheng, J. T. J.; Hancock, R. E. W.; Straus, S. K. Structural Studies of a Peptide with Immune Modulating and Direct Antimicrobial Activity. *Chem. Biol.* **2010**, *17*, 970−980.
(69) Kyte, J.; Doolittle, R. F. A simple method for displaying the hydropathic character of a protein. *J. Mol. Biol.* **1982**, *157*, 105−132.